applied optics

Phase shifting interferometry using a spatial light modulator to measure optical thin films

Brenda Villalobos-Mendoza,[1,*] Fermín S. Granados-Agustín,[1] Daniel Aguirre-Aguirre,[1,2] and Alejandro Cornejo-Rodríguez[1]

[1]Instituto Nacional de Astrofísica Óptica y Electrónica, Optics Departament, Luis Enrique Erro No. 1, C. P. 72840, Santa María Tonantzintla, Puebla, Mexico
[2]Centro de Ciencias Aplicadas y Desarrollo Tecnológico, Universidad Nacional Autónoma de México, Circuito Exterior S/N, Apartado Postal 70-186, D. F. 04510, Mexico
*Corresponding author: bvillalobosmendoza@gmail.com

Received 26 February 2015; revised 14 August 2015; accepted 19 August 2015; posted 20 August 2015 (Doc. ID 242837); published 10 September 2015

This work describes a process for measuring thin film steps, using phase shifting interferometry (PSI). The phase shifts are applied only in the region where the thin film steps are located. The phase shift is achieved by displaying different gray levels on a spatial light modulator (SLM Holoeye LC2012) placed in one arm of a Twyman–Green (T–G) interferometer. Before measuring the thin film steps, it was necessary to quantify the phase shifts achieved with this SLM by measuring the fringe shifts in experimental interferograms. The phase shifts observed in the interference patterns were produced by displaying the different gray levels on the SLM one by one, from 0 to 255. The experimental interferograms and the thicknesses of the thin film steps were successfully quantified, proving that this method can be used to measure thin films by applying the PSI method only on the region occupied by them.

OCIS codes: (050.5080) Phase shift; (240.0310) Thin films; (230.6120) Spatial light modulators.

http://dx.doi.org/10.1364/AO.54.007997

1. INTRODUCTION

The use of spatial light modulators based on liquid crystals is becoming more common to modulate either the amplitude or the phase of light [1–3]. In the field of optical testing, an example of the use of this kind of spatial light modulator (SLM) for amplitude modulation is the Ronchi test, where instead of using a classical Ronchi ruling (engraved on a photographic plate), the SLM are used to display different types of rulings for testing optical surfaces [4–7]. In the case of phase modulation, SLMs have been widely adopted in the field of control beams, pulsed laser systems [8,9], and adaptive optics [10,11].

In this work, we propose the use of these SLMs for measuring local thin film steps by shifting the phase only in the region occupied by the local step, taking advantage of the pixel configuration of the SLM. The phase shifts are performed by placing the SLM in one arm of a Twyman–Green (T–G) interferometer and applying different gray levels to the SLM. As a first step, we obtained the phase shift curve for the SLM Holoeye LC2012.

The techniques used to measure the phase introduced by these SLMs are varied. One of the methods, for example, is phase "extraction," which uses an intensity correlation matrix to determine the phase [12]. Interferometry is one of the most used experimental techniques for calibrating a SLM [13,14].

In our case, the phase shift curve of the SLM was obtained by displaying different gray level images on the SLM. Each image was divided in two equal parts: the upper part with varying gray levels from 0 to 255, and the lower part with a fixed gray level of zero as reference. This reference allowed us to find the phase shift of the interference fringes introduced by the different gray levels of the SLM. The image of the shifted interferogram was recorded at the same time. Finally, this work reports a reliable technique for measuring the thicknesses of optical thin films using a SLM.

2. INTENSITY FUNCTION OF A MICHELSON INTERFEROMETER

Since our interest was to obtain the curve "phase shift versus gray level" by means of a SLM, we used a Michelson interferometer. There are three principal measurements that can be made with the Michelson interferometer: (1) the width and fine structure of a spectral line, (2) the length or displacement in terms of the wavelength of light, and (3) the refractive index [14].

When a Michelson interferometer is illuminated with strictly monochromatic light, produced by a point source, it becomes a very powerful instrument for testing optical surfaces. This instrument is known as a T–G interferometer [13].

Therefore, it is important to know the intensity function generated by the interference of two waves produced in the Michelson interferometer. This is achieved by superimposing two wavefronts: one a typically flat reference wavefront and the other a distorted wavefront [13]. The irradiance $I(x,y)$ at any point in an interferogram can be expressed as a function of the light source wavelength and the optical path difference (OPD) between the two interfering wavefronts as [15]

$$I(x,y) = a(x,y) + b(x,y)\cos\left(\frac{2\pi \mathrm{OPD}}{\lambda} + \Delta\phi\right), \quad \textbf{(1)}$$

where $a(x,y)$ and $b(x,y)$ are background intensity and local contrast, respectively, λ is the light source wavelength, and $\Delta\phi$ is the phase shift associated with the gray level displayed on the SLM.

The OPD in a Michelson interferometer [16] is $n_0 2d\cos\theta$, which represents a phase difference of $k_0 n_0 2d\cos\theta$. Destructive interference will exist when

$$n_0 2d\cos\theta_m = m\lambda_o, \quad \textbf{(2)}$$

where m is an integer. If we use a source containing a number of different frequency components (e.g., a white light source), the dependence of θ_m on λ_0 in Eq. (2) requires that each of those components generates a fringe system of its own [16–18].

Notice that a central dark fringe for which $\theta_m = 0$ in Eq. (1) can be represented by $2d = m_0\lambda_0$, and this dark fringe will be used as reference position to find the phase shift of the fringes when a T–G interferometer is used.

3. EXPERIMENTAL SETUP

White light fringes are used in the Michelson interferometer to locate the position of zero path difference, and they are used to recognize a reference fringe in the monochromatic pattern [18]. Therefore, as a first step, we used the Michelson interferometer and a white lamp, achieving the same optical path for the two arms of the interferometer, as shown in Fig. 1. The second step was to convert the Michelson interferometer into a T–G interferometer, in which two kinds of light are used (a white lamp and a diode laser with $\lambda = 532$ nm), the spatial filter was a combination of a microscope objective of 40X and a pinhole with a diameter of 10 μm, a cube beam splitter 50/50, two flat mirrors with $\lambda/4$, and a CMOS detector PixeLink PL-B776 with a resolution of 2048 × 1536 pixels.

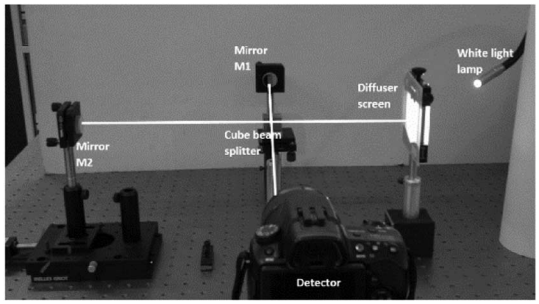

Fig. 1. Michelson interferometer with a white light source.

When the Michelson interferometer is converted into a T–G interferometer, there are, in general, straight line fringes parallel to the apex of the wedge. On the other hand, because of the departure from monochromatism of the source, the fringes are visible only if the optical paths in the two arms are sufficiently near to equality. Thus, it is very important to achieve the same path in the Michelson interferometer before converting it into a T–G interferometer [18].

Since a SLM was placed in one of the arms of our version of the T–G interferometer, the white light fringes pattern disappears and the change in the optical path produced by the thickness of the SLM had to be compensated by displacing the mirror of the other arm of the interferometer until recovering again the white light fringes pattern. This calibration is important because it is necessary to ensure that the fringe shifts observed in the experimental interferograms are produced by the gray levels displayed in the SLM and not by the thickness of the SLM.

To obtain the fringe shifting using the experimental setup of Fig. 2, different gray levels were displayed on the SLM, from 0 to 255. To do this, we developed an algorithm that modified the image with different gray levels displayed on the SLM.

The algorithm, which will be explained in detail in Section 4, generates an image with the same size of the SLM resolution (1024 × 768). This image matrix is divided in sections with different gray levels. When every gray level is displayed on the SLM, a change in the phase of the wavefront results in a fringe shift in the experimental interferogram recorded with the detector.

Figure 3 shows the shifting effect produced by gray level changes on the interference pattern recorded by the detector.

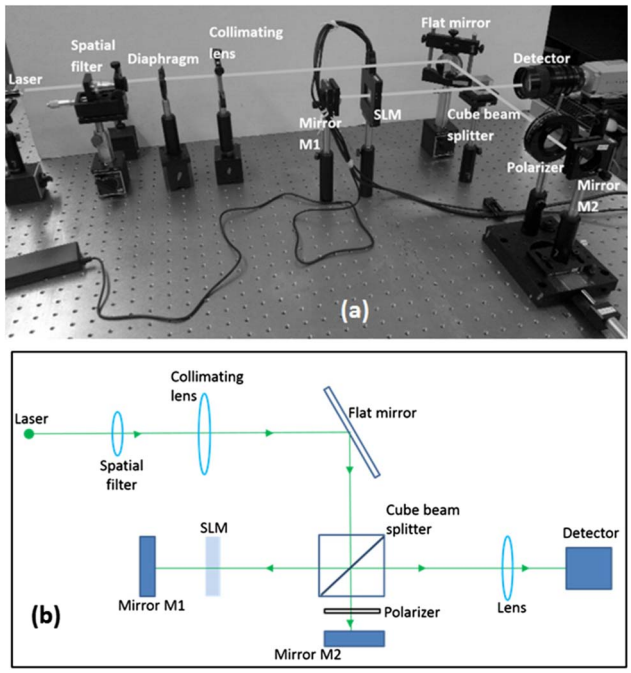

Fig. 2. Twyman–Green (T–G) fringe shifting. (a) Experimental set up and (b) scheme of the experimental set up.

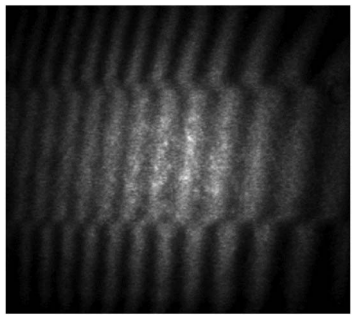

Fig. 3. Testing the SLM.

This analysis showed that when different gray levels are displayed on the SLM, it produces a fringe shift in the experimental interferogram recorded by the detector. With this result, the next step was to measure the phase shift for every gray level.

Figure 4 shows some examples of the phase-shifted interferograms with their corresponding gray level. A qualitative analysis of the interferograms showed a noticeable phase shift until the 40th gray level was applied to the SLM; a total 2π shift was produced between the first and the last interferogram.

In order to improve the fringe shift observed in the interferograms, the gray levels of the SLM were divided in such a way that the lower part of the images maintained a gray level of zero, while the upper part showed different gray levels. Figure 5 shows two examples of the interferogram images recorded with the detector for two different gray levels on the upper part.

It is worth noting, with respect to the zero gray level used as reference value (Fig. 5), the fact that turbulence effects for each phase-shifted interferogram were recorded at the same time for the reference and the phase-shifted interferogram, and that the interference fringes were moving from left to right.

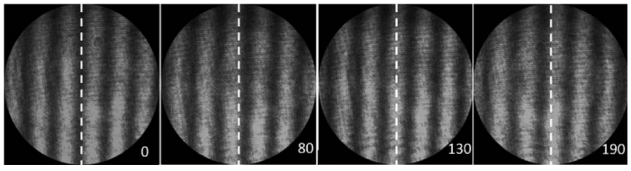

Fig. 4. Experimental interferograms corresponding to every gray level displayed on the SLM.

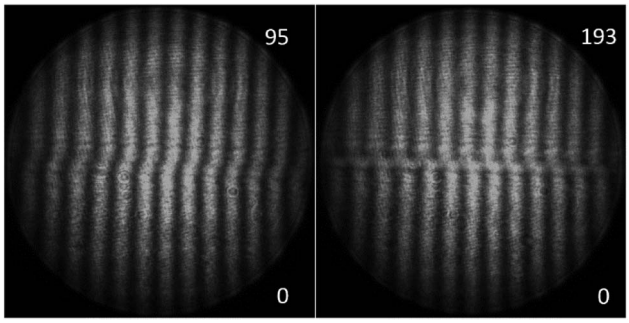

Fig. 5. Experimental interferograms using a reference gray value in the images displayed on the SLM for two different gray levels.

4. ALGORITHM FOR FRINGE SHIFTING ON THE SLM

In order to obtain quantitative values of the phase shifts introduced in the original interferograms by changing the gray levels of the SLM using the experimental setup of Fig. 2, we used an algorithm to find the association between the fringe shifts and the changes in the gray levels of the SLM. Figure 6 shows the block diagram of the algorithm developed to improve finding the positions of the interferogram fringes.

The algorithm comprises four cycles. The first cycle reads all recorded experimental interferograms. The second cycle performs a smoothing of every read interferogram and applies an "average" filter in the desired neighborhood [19]. Figure 7 shows an example of an image profile obtained in this cycle. The result of this cycle is an image with the same size as that of the input image but smoother and with less noise.

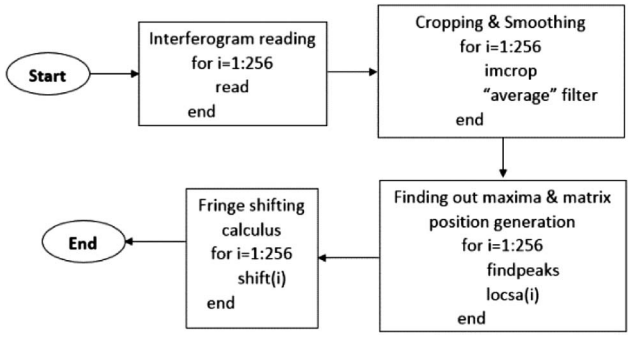

Fig. 6. Block diagram of the algorithm.

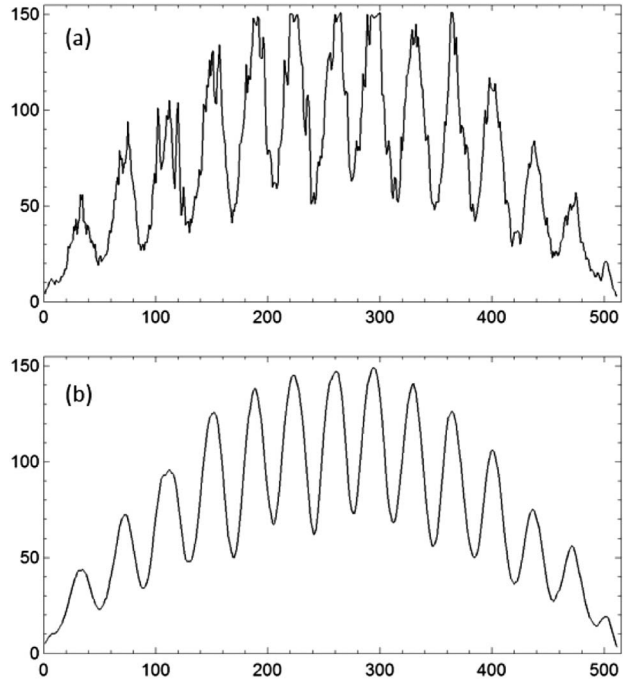

Fig. 7. Central profiles of the experimental interferograms. (a) Image without smoothing and (b) the smooth image.

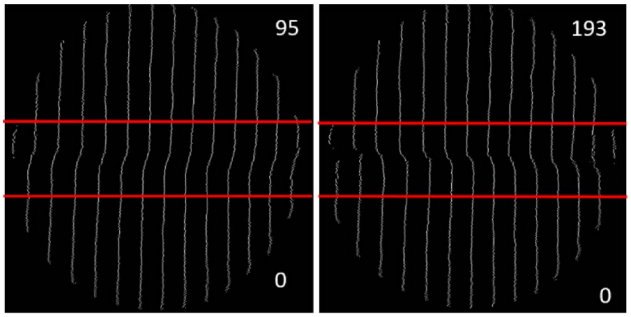

Fig. 8. Centroids of the experimental interferograms for two different gray levels.

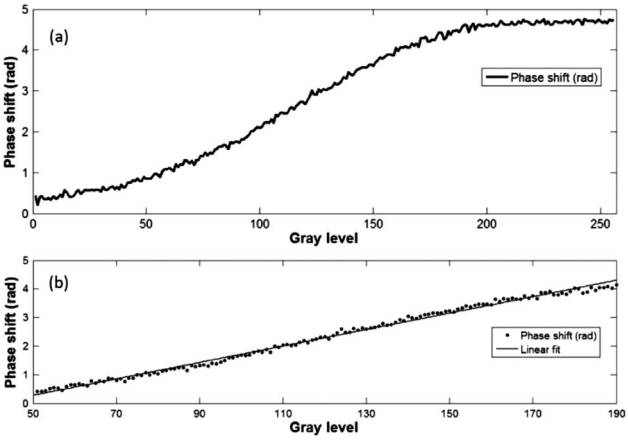

Fig. 9. Phase shifts introduced by each gray level. (a) Gray levels from 0 to 255 and (b) linear fit between the 50th and the 190th gray levels.

The third block shown in Fig. 6 is the most important of all because it is the cycle whose function is to find the maximum value and position of each fringe in the analyzed interferogram; this is done by comparing every pixel with its neighbors. If the value of one pixel is greater than its neighbor, it is considered as the local maximum and saved. This process is repeated for all pixels of every image row. Figure 8 shows some examples of the skeleton interferograms.

The last step of the algorithm (the fourth block of Fig. 6) makes a comparison of the fringe position between two neighboring rows; one row from the lower reference interferogram of Fig. 8, and the other row corresponding to the upper interferogram with a phase shift introduced by varying the gray level on the SLM. This process was done for all 256 interferograms recorded and gave us the shifts introduced by the variations of every gray level displayed in the SLM. Figure 9 shows a graph corresponding to the phase shifts produced by changing the gray levels on the SLM from zero (reference) to 255.

5. CALCULATION OF THE "PHASE SHIFT VERSUS GRAY LEVEL" CURVE

Once the interferograms were as those shown in Fig. 8, by means of the fourth block of the algorithm shown in Fig. 6, we obtained the curve of Fig. 9 by analyzing two lines perpendicular to the fringes of the upper and bottom interferograms of Fig. 8 by counting the shift introduced by the gray levels on the SLM. The upper line corresponds to the part of the interferogram where the gray level changed from 0 to 255, while the lower line corresponds to the part of the interferogram where the gray level remained fixed in the reference value of zero. The point where each fringe crossed the line on each interferogram of Fig. 8 allowed us to know the position in pixels. By comparing the crossing points for both interferograms, it was possible to know the fringe shift between the different gray levels with respect to the zero value.

The above procedure used to determine the fringe shift was performed for each of the 256 interferograms. To quantify the phase shift value in radians, the phase between two maxima was 2π, while the distance in pixels corresponding to 2π was 36. This value of 36 is derived from the average for the 256 interferograms.

An important result from the graphic of Fig. 9 is that the region between the 50th and the 190th gray levels is where the best results can be obtained when introducing phase shifts by changing the gray levels in the SLM, with a standard deviation of 0.0920 and an uncertainty value of ± 0.168 rad. Another important aspect of the obtained phase shift graphic is that the observed noise is the result of the noise that is present and inherent in every experimental image captured in the laboratory. However, as can be seen in Fig. 9, the graphic is almost smooth because an average was calculated for all the shifts of every maximum value in the interference pattern before obtaining these results.

6. THIN FILM STEPS: EXPERIMENTAL MEASUREMENTS USING THE SLM

The thin film steps were deposited on a flat surface with a rms $= \lambda/28$ and a peak-to-valley of $P - V = \lambda/4$. As can be seen in Fig. 9, it is possible to measure phase shifts $\approx 1.5\pi$. Thus, the thicknesses of the thin film steps were chosen to produce phase shifts according to the phase shift curve obtained with the SLM. The characteristics of the thin film deposited and measured are the next ones: the material was magnesium fluoride with an index refraction of 1.38 and a thickness of $\lambda/4$ over a BK7 glass used as a substrate. The value of $\lambda/4$ was measured with the system in the Balzers vacuum chamber of the Institute, model BA-510. As a matter of fact, the difference between the index refraction of the thin film and the substrate is equal to 0.13.

The main aim of the technique proposed in this work is the measurement of thin films used for antireflection coatings; its use for other materials will be done in the near future, with applications in the field of electronics. The deposited thin film steps had phase shifts of $\pi/2$, π and $3\pi/2$. Figure 10 shows an interferogram in which the three thin film steps of the surface under test can be seen. Note that the steps of the thin film were deposited on the central region of the surface under test. Thus, there were no thin films on either of the two edges.

According to the experimental setup shown in Fig. 2, the M1 mirror was substituted by the surface with thin films to measure the deposited thin film steps. Three experimental

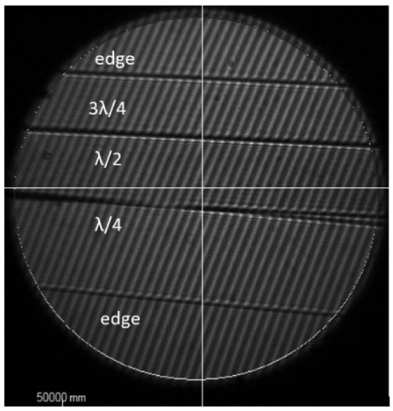

Fig. 10. Steps of the surface under test.

interferograms corresponding to each thin film step were then recorded. In order to select the gray level that best fits the step, all the gray levels were displayed on the SLM one by one until the fringes in the interferogram were aligned. Afterward, two more interferograms were recorded: one above and one below the best gray level. Figure 11 shows two experimental interferograms, with one before compensating the step and the other after the step was compensated.

In order to evaluate the RMS and determine the best compensated gray level, we used the least squares algorithm to find the best-fit line corresponding to each fringe in the experimental interferograms.

To find the least squares best-fit line, we had to minimize the quantity

$$E = [y_1 - (a_0 + a_1x_1)]^2 + [y_2 - (a_0 + a_2x_2)]^2 + \ldots + [y_n - (a_0 + a_nx_n)]^2, \quad (3)$$

where E is the least squares error [20]. To find the least squares line we have

$$v_1 = \begin{bmatrix} 1 \\ 1 \\ \vdots \\ 1 \end{bmatrix}, \quad v_2 = \begin{bmatrix} x_1 \\ x_2 \\ \vdots \\ x_n \end{bmatrix}, \quad y = \begin{bmatrix} y_1 \\ y_2 \\ \vdots \\ y_n \end{bmatrix} \quad \text{and}$$

$$C = [v_1, v_2]. \quad (4)$$

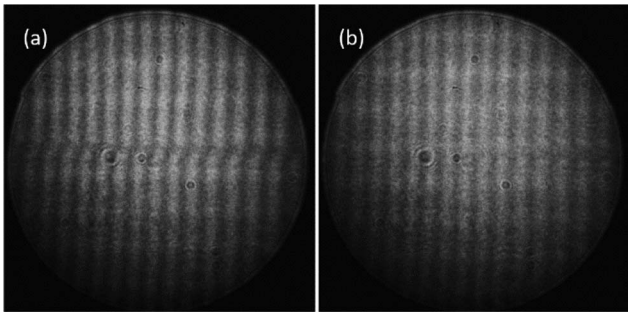

Fig. 11. Surface with steps. Experimental interferograms (a) without compensation and (b) with compensation.

To minimize E, it is necessary to find a vector that obeys

$$a_0v_1 + a_1v_2 = C\begin{bmatrix} a_0 \\ a_1 \end{bmatrix}, \quad (5)$$

where the best fit occurs when $\left[\begin{smallmatrix} a_0 \\ a_1 \end{smallmatrix}\right]$ is a solution to the normal equations system. Given that C^TC is an invertible matrix, it can be seen that the least squares line has the form

$$y = a_0 + a_1x, \quad (6)$$

where

$$\begin{bmatrix} a_0 \\ a_1 \end{bmatrix} = (C^TC)^{-1}C^Ty. \quad (7)$$

To find the gray level that best fits the step, first the centroids of the experimental interferograms were calculated (Fig. 12). Then, the least squares algorithm for the best fit-line was applied to the centroid of each fringe in the experimental interferogram; see Fig. 13. After this fit was done, we calculated its RMS to determine the best fit to compensate the step in the surface under test using [21]

$$\text{RMS} = \sqrt{\frac{1}{n}\sum (y_t - y_o)^2}. \quad (8)$$

When the best gray level has been chosen by means of the RMS and according with the graph of Fig. 9, the thickness corresponding to the gray level was picked and taken as the thickness of the step for the step between the edge and $\lambda/4$ the 109 gray level, for the step between $\lambda/4$ and $\lambda/2$ the 99 gray level,

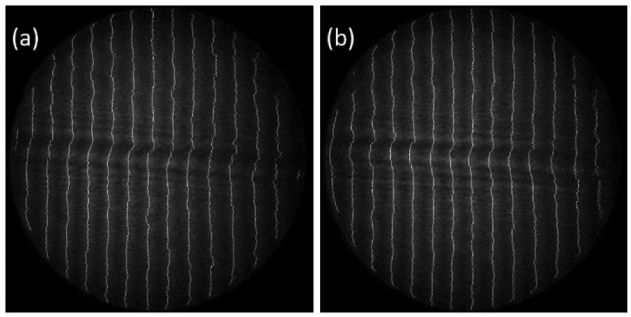

Fig. 12. Overlap between the experimental interferograms with their centroids. (a) Without compensation and (b) with compensation.

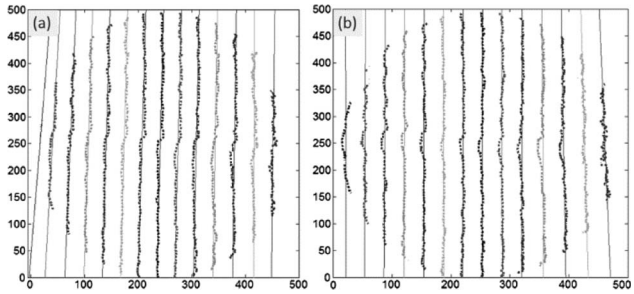

Fig. 13. Least squares algorithm applied to the centroids of the experimental interferograms. (a) Without compensation and (b) with compensation.

Table 1. Expected Step Thickness

Step	Expected Thickness (μm)	Thickness Measured with the SLM (μm)
Edge and $\lambda/4$	0.1582	0.1740
$\lambda/4$ and $\lambda/2$	0.3164	0.3152
$\lambda/2$ and $3\lambda/4$	0.4746	0.4580

and for the step between $\lambda/2$ and $3\lambda/4$ the 100 gray level. Table 1 shows the thickness of every thin film step according to the each best-fit gray level.

The expected thickness for each step was obtained from McLeod [22]. This design program calculates each thin film according to the material deposited in the substrate under test.

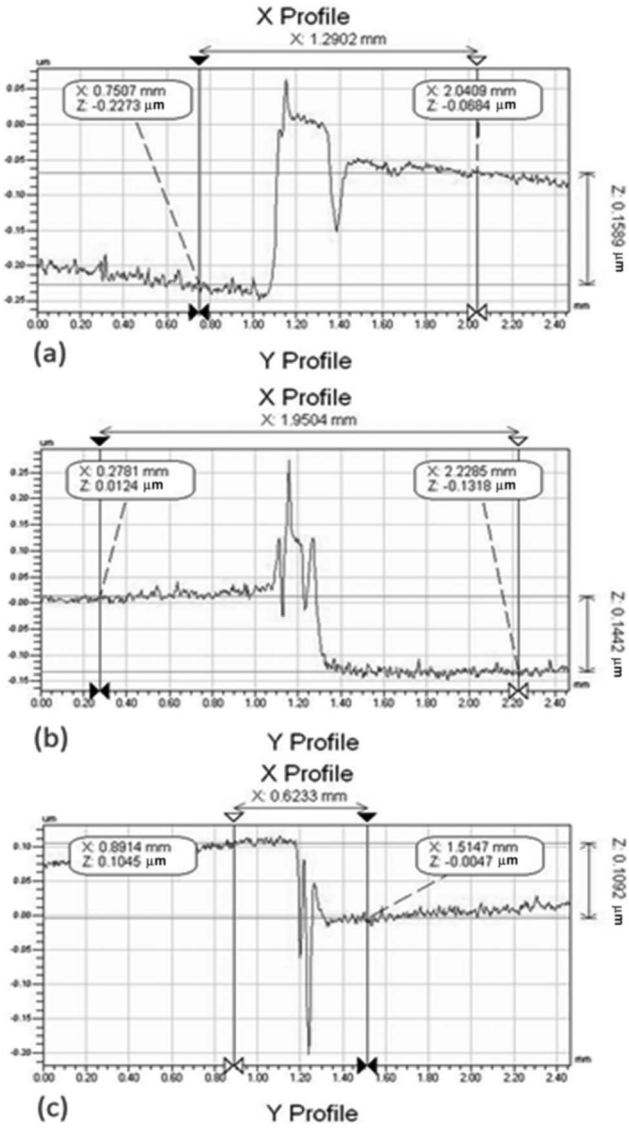

Fig. 14. Profiles measured using a microscopic interferometer WYKO. (a) Step of edge and $\lambda/4$, (b) step of $\lambda/4$ and $\lambda/2$, and (c) step of $\lambda/2$ and $3\lambda/4$.

Table 2. Comparison of Step Thickness of WYKO and SLM

Step	Expected Thickness (μm)	Thickness Measured with the SLM (μm)	Thickness Measured with WYKO (μm)
$\lambda/4$	0.1582	0.1740	0.1589
$\lambda/2$	0.3164	0.3152	0.3031
$3\lambda/4$	0.4746	0.4580	0.4123

7. COMPARISON BETWEEN WYKO AND THE PROPOSED TECHNIQUE

To verify the results obtained with our method, we performed a second measuring of the thin film steps with an interferometric microscope WYKO. The WYKO NT1100 is an optical profiler providing three-dimensional surface profile measurements without contact. Two working modes are available: VSI vertical shift interference (VSI) and phase shift interference (PSI). We used the VSI mode, based on white light vertical scanning interferometry. The maximum measurable topography is 1 mm and there are some limitations for measuring slopes, depending on the optical numerical aperture and the surface roughness [23].

The thin film steps were measured by regions in the WYKO interferometric microscope due to its spatial resolution, which depends on the objective magnification used (20 × –4.7 mm and 50 × –3.4 mm). The three thin film profiles that were measured are shown in Fig. 14. The first measurement was made with respect to the edge of the surface under test. The other two measurements were done between each step. Thus, to obtain the real thickness of the second step it is necessary to sum the first measurement, while for the third step it is necessary to sum the first, second, and third measurements. The real thicknesses of every measured step are shown in Table 2.

8. CONCLUSIONS

This work described a process used to obtain the curve "phase shift versus gray level" of the SLM Holoeye LC2012. This process can be used to produce phase shifts in interferometry and to quantify the phase shifts in deposited thin films. The main work done with the SLM was changing the values of the gray levels directly on the images. After obtaining and calibrating the changes in the gray levels, they were applied to the phase shifts observed in experimental interferograms, observing the shifts introduced to the positions of the interference fringes (Fig. 9). Before obtaining quantitative and qualitative results of the amount of phase shifting introduced in an interferogram, it was necessary to know the reference position. This was done by means of the classical Michelson interferometer, with equal optical paths for both arms of the interferometer. From the analysis done using the SLM, we determined that the best working range of this device was between the 50th and the 190th gray levels, with a deviation standard of 0.0920 in the phase shifts and an uncertainty value of ±0.168 rad.

Acknowledgment. We thank Dr. Francisco Renero for allowing to use the WYKO interferometric microscope. We

thank Pedro Técuatl Técuatl and Magdalena Hernández, INAOE's technicians, for the aluminization and deposition of the thin films.

REFERENCES

1. M. S. Mahmud, I. Naydenova, and V. Toal, "Implementation of phase-only modulation utilizing a twisted nematic liquid crystal spatial light modulator," J. Opt. A **10**, 085007 (2008).
2. L. Hu, L. Xuan, Y. Liu, Z. Cao, D. Li, and Q. Mu, "Phase-only liquid-crystal spatial light modulator for wave-front correction with high precision," Opt. Express **12**, 6403–6409 (2004).
3. S. H. Eng, D. M. Cai, Z. Wang, K. Alameh, and W. Jiang, "Optimization of liquid-crystal spatial light modulator for precise phase generation," in *Proceeding IEEE Conference of Optoelectronic and Microelectronic Materials and Devices*, Perth, Australia, 2006, pp. 105–108.
4. M. Mora-González and N. Alcalá-Ochoa, "Flatness measurement by a grazing Ronchi test," Opt. Commun. **191**, 203–207 (2001).
5. J. Castro-Ramos, S. Vázquez-Montiel, and A. Padilla-Vivanco, "Phase shifting interferometry by using a LCD and Bironchi test," Proc. SPIE **5662**, 639–645 (2004).
6. M. Mora-González and N. Acalá-Ochoa, "Sinusoidal liquid crystal display grating in the Ronchi test," Opt. Eng. **42**, 1725–1729 (2003).
7. D. Aguirre-Aguirre, F. Granados-Agustín, M. Campos-García, and A. Cornejo-Rodríguez, "Evaluation of the increment of the sampling in optical testing using sub-structured Ronchi gratings," J. Phys. **274**, 012062 (2011).
8. Y. Liu, L. Xuan, L. Hu, Z. Cao, D. Li, Q. Mu, and X. Lu, "Investigation on the liquid crystal spatial light modulator with high precision and pure phase," Acta Opt. Sin. **25**, 1682–1686 (2005).
9. X. Chu, S. Zhan, S. Zhao, Y. Li, and J. Xu, "Research on phase-detecting method for coherent beam combining of fiber laser array," Optoelectron. Lett. **3**, 455–458 (2008).
10. C. Li, M. Xia, Q. Mu, B. Jiang, L. Xuan, and Z. Cao, "High-precision open-loop adaptive optics system based on LC-SLM," Opt. Express **17**, 10774–10781 (2009).
11. G. Love, "Wave-front correction and production of Zernike modes with a liquid-crystal spatial light modulator," Appl. Opt. **36**, 1517–1524 (1997).
12. H. Yue, L. Song, Z. Hu, H. Liu, Y. Liu, Y. Liu, and Z. Peng, "Characterization of the phase modulation property of a free-space electro-optic modulator by interframe intensity correlation matrix," Appl. Opt. **51**, 4457–4462 (2012)
13. D. Malacara, *Optical Shop Testing*, 2nd ed. (Taylor & Francis, 2005).
14. L. Z. Cai, Q. Liu, and X. L. Yang, "Phase-shift extraction and wave-front reconstruction in phase-shifting interferometry with arbitrary phase steps," Opt. Lett. **28**, 1808–1810 (2003).
15. W. S. Meyers and H. P. Stahl, "Sensitivity of two-channel Ronchi test to grating misalignment," Proc. SPIE **1994**, 90–101 (1994).
16. E. Hecht, *Optics*, 4th ed. (Pearson, 2001).
17. T. Li, A. Wang, K. Murphy, and R. Claus, "White-light scanning fiber Michelson interferometer for absolute position-distance measurement," Opt. Lett. **20**, 785–787 (1995).
18. M. Born and E. Wolf, *Principles of Optics*, 6th ed. (Pergamon, 1980).
19. D. Malacara, M. Servín, and Z. Malacara, *Interferogram Analysis for Optical Testing*, 2nd ed. (Taylor & Francis, 2005).
20. S. Roman, *Advanced Linear Algebra*, 3rd ed. (Springer, 2008).
21. R. E. Walpole, R. H. Myers, S. L. Myers, and K. Ye, *Probability and Statistics for Engineers and Scientists*, 9th ed. (Prentice Hall, 2012).
22. http://www.thinfilmcenter.com/essential.html, 2014.
23. https://cmi.epfl.ch/metrology/Wyko_NT1100.php, 2014.